The Astrophysical Journal, 741:49 (10pp), 2011 November 1 doi:10.1088/0004-637X/741/1/49

A COMPLETE SAMPLE OF ULTRALUMINOUS X-RAY SOURCE HOST GALAXIES

Douglas A. Swartz[1], Roberto Soria[2], Allyn F. Tennant[3], and Mihoko Yukita[4]
[1] Universities Space Research Association, NASA Marshall Space Flight Center, VP62, Huntsville, AL 35812, USA
[2] Curtin Institute of Radio Astronomy, Curtin University, 1 Turner Avenue, Bentley, WA 6102, Australia
[3] Space Science Office, NASA Marshall Space Flight Center, VP62, Huntsville, AL 35812, USA
[4] Department of Physics & Astronomy, University of Alabama, Tuscaloosa, AL 35487, USA
Received 2011 June 29; accepted 2011 August 3; published 2011 October 14

ABSTRACT

One hundred seven ultraluminous X-ray sources (ULXs) with 0.3–10.0 keV luminosities in excess of 10^{39} erg s^{-1} are identified in a complete sample of 127 nearby galaxies. The sample includes all galaxies within 14.5 Mpc above the completeness limits of both the Uppsala Galaxy Catalogue and the *Infrared Astronomical Satellite* survey. The galaxy sample spans all Hubble types, a four-decade range in mass, $7.5 < \log(M/M_\odot) < 11.4$, and in star formation rate, $0.0002 < \mathrm{SFR}(M_\odot\ \mathrm{yr}^{-1}) \leqslant 3.6$. ULXs are detected in this sample at rates of one per $3.2 \times 10^{10}\ M_\odot$, one per $\sim 0.5\ M_\odot\ \mathrm{yr}^{-1}$ star formation rate, and one per 57 Mpc^3 corresponding to a luminosity density of $\sim 2 \times 10^{37}$ erg s^{-1} Mpc^{-3}. At these rates we estimate as many as 19 additional ULXs remain undetected in fainter dwarf galaxies within the survey volume. An estimated 14 objects, or 13%, of the 107 ULX candidates are expected to be background sources. The differential ULX luminosity function shows a power-law slope $\alpha \sim -0.8$ to -2.0 with an exponential cutoff at $\sim 20 \times 10^{39}$ erg s^{-1} with precise values depending on the model and on whether the ULX luminosities are estimated from their observed numbers of counts or, for a subset of candidates, from their spectral shapes. Extrapolating the observed luminosity function predicts at most one very luminous ULX, $L_X \sim 10^{41}$ erg s^{-1}, within a distance as small as 100 Mpc. The luminosity distribution of ULXs within the local universe cannot account for the recent claims of luminosities in excess of 2×10^{41} erg s^{-1}, requiring a new population class to explain these extreme objects.

Key words: galaxies: general – surveys – X-rays: binaries – X-rays: galaxies – X-rays: general

Online-only material: color figure

1. INTRODUCTION

Ultraluminous X-ray sources (ULXs) are defined as non-nuclear point-like objects in external galaxies, with apparent isotropic X-ray luminosity higher than that of stellar-mass Galactic black holes: typically, $L_X > 10^{39}$ erg s^{-1} in the 0.3–10 keV band. By this empirical definition, ULXs may encompass extreme examples of high-mass and low-mass X-ray binaries, recent supernovae, rotation-powered young pulsars, and perhaps intermediate-mass black holes. In practice, supernovae are excluded, and high-energy pulsars are not expected to be a significant population at these luminosities (Perna & Stella 2004; Perna et al. 2008). So, the study of ULXs concentrates exclusively on accretion systems. Blazar-like beaming is ruled out for at least some of the brightest sources; hence the consensus is that most ULXs do have high luminosities and high mass accretion rates. This has led to two diverging scenarios with circumstantial observational support: (1) near-Eddington or moderately super-Eddington sources powered by stellar black holes, $M \lesssim 80\ M_\odot$; (2) sub-Eddington sources powered by high mass accretors, with $M \gtrsim 100\ M_\odot$. In scenario (1), the high accretion rate implies that standard thin-disk models are not appropriate and have to be replaced by geometrically thicker disks (e.g., slim disks; Abramowicz et al. 1988; Kawaguchi 2003; Poutanen et al. 2007; Gladstone et al. 2009) with massive outflows.[5] This introduces the possibility of mild geometrical beaming inside a conical outflow (King 2009, and references therein), which would reduce the required black hole mass and the need to violate the classical Eddington limit. The accreting intermediate-mass black holes of scenario (2) might come from Pop III stars (Madau & Rees 2001), from the collapsed core of young, massive star clusters or molecular cores (Portegies Zwart et al. 2004), or from the nucleus of accreted satellite galaxies (King & Dehnen 2005). But the likelihood that such exotic objects can capture a donor star and form an X-ray luminous system is low (Baumgardt et al. 2006; Madhusudhan et al. 2006).

Ultimately, the question we want to answer is as follows: are ULXs an extreme example of well-known X-ray binaries (the high accretion rate and high black hole mass tail of the X-ray binary distribution), or do they require a new, physically distinct, population of accreting black holes not formed from single-star processes in the current epoch? We do not have direct estimates of black hole masses with which these two scenarios could be distinguished. Since X-ray luminosity is the defining property of this class, and probably the least model-dependent quantity, the question we ask instead is whether there is a maximum ULX luminosity. If ULXs are powered by stellar black holes, we expect their maximum luminosity to be at $L_X \sim 10^{40}$ erg s^{-1} within a factor of a few corresponding to the Eddington limit of the maximum stellar black hole mass. If ULXs are powered by sub-Eddington intermediate-mass black holes, we expect luminosities of $\sim 10^{42}$ erg s^{-1} and above for black hole masses $\gtrsim 10^4\ M_\odot$.

Moreover, the same L_X requires different mass accretion rates in the two scenarios, and hence we predict a different lifetime of the brightest sources. For super-Eddington sources, $L_X \propto L_{\mathrm{Edd}}(1 + \frac{3}{5}\ln(\dot{M}/\dot{M}_{\mathrm{Edd}}))$; a luminosity $L_X \sim 10^{40}$ erg s^{-1} requires $\dot{M} \sim 2 \times 10^{-5}\ M_\odot\ \mathrm{yr}^{-1}$ if coming from a $25\ M_\odot$

[5] Hence, the standard disk scaling relations between temperature, luminosity, and black hole mass, well tested for (sub-Eddington) Galactic black holes, would not be applicable to ULXs.

black hole. For sub-Eddington sources, $L_X \propto 0.1\dot{M}c^2$; the same luminosity $L_X \sim 10^{40}$ erg s^{-1} requires an accretion rate of only $\dot{M} \sim 2 \times 10^{-6}\, M_\odot$ yr^{-1} for black hole masses $>100\, M_\odot$.

Of course, the luminosity of X-ray binaries is rarely steady; one cannot equate a single observed luminosity of a particular object to a definite mass with any certainty. But, if ULXs *as a class* are powered by stellar-mass black holes, then the high end of their luminosity distribution would have a sharp downturn because of the combined effect of upper black hole mass limit and shorter active lifetime. Conversely, if ULXs are intermediate-mass black holes, then no luminosity cutoff would be expected.

The best approach to addressing these predictions is to study a large sample of ULXs in a variety of galaxies in order to determine their luminosity distribution. An ideal survey would include every galaxy within a fixed distance. Once the ULX phenomena are understood and quantified within such a complete sample, the results can be extended to studies of more distant objects where only the integrated X-ray light from entire galaxies can be measured. This is the goal of the present study. Unfortunately, there are no measurements that go deep enough to catalog all the low-mass dwarf galaxies out to a reasonable distance. We can still achieve most of the scientific advantages of a complete survey by accounting for the missing population by using well-defined and quantifiable selection criteria. Thus, our aim is to produce a statistically rigorous sample of ULX candidates, to provide precise astrometric positions, and to estimate their X-ray luminosities using a carefully defined sample of nearby galaxies.

The survey galaxy sample is defined in Section 2. The data and data analysis methods used in this study are described in Section 3. The results of the analysis are presented in Section 4, including analysis of the sample completeness, a census of ULX candidates, some of their properties with respect to their host galaxies, and their luminosity distribution function. Section 5 discusses the results.

2. SAMPLE DEFINITION

We began with a list of all galaxies within 14.5 Mpc contained in the Uppsala Galaxy Catalogue (UGC) with photographic magnitude within the Catalogue's completeness limit of $m_p < 14.5$ mag. The UGC (Nilson 1973) contains all galaxies north of B1950 $\delta = -2^\circ 30'$ in both of two complete samples: galaxies with angular diameters $>1'$ on the first POSS blue prints and galaxies brighter than $m_p = 14.5$ mag in the Zwicky Catalog of Galaxies and Clusters of Galaxies. The distance restriction was chosen to ensure that any additional *Chandra* X-ray observations needed to complete the survey require integration times of $\leqslant 5$ ks in order to detect 20 counts ($>3\sigma$ S/N) in the 0.3–6.0 keV *Chandra* band from a source with a luminosity of 10^{39} erg s^{-1} at the distance of the target galaxy. This resulted in a sample of 266 galaxies. We then eliminated those galaxies below the completeness limit of the *Infrared Astronomical Satellite (IRAS)* survey, $\sim$1.5 Jy at 60 μm (Beichman et al. 1988). This eliminates galaxies with low star formation rates (SFRs) which are known to host few, if any, ULXs (e.g., Grimm et al. 2003; Ranalli et al. 2003). The final sample consists of 127 galaxies.

This sample was compared to a compilation extracted from the NASA/IPAC Extragalactic Database (NED) of all objects designated as a galaxy with Virgo-infall velocity $\leqslant 1060$ km s^{-1} (corresponding to $\sim$14.5 Mpc for $H_o = 73$ km s^{-1}), and with declination above $\delta = -2.^\circ 5$ (B1950). This compilation contained about 760 objects of which 173 met the UGC and *IRAS* constraints imposed on angular size, optical magnitude, and far-IR flux. The differences between this compilation and our sample are ascribed to differences in the distance estimates (see Section 3.1). For reference, of the 760 objects, 579 are below the *IRAS* flux completeness criterion, 364 fail the UGC photographic completeness criterion, and 34 are smaller than $1'$ diameter.

3. PROPERTIES OF ULX CANDIDATES AND ANCILLARY DATA

Most of the galaxies in the present sample have been observed with the *Chandra X-Ray Observatory* Advanced CCD Imaging Spectrometer (ACIS). For consistency, *Chandra*/ACIS data have been used for analysis when available unless a much deeper *XMM-Newton* observation exists (even then, *Chandra* data were used to locate X-ray sources if the observation was judged deep enough to detect ULXs at $>3\sigma$ significance). For galaxies with multiple exposures, the deepest exposure imaging the full optical extent of the target galaxy was analyzed unless the target was previously analyzed by Swartz et al. (2004, hereafter S04), in which case our original work was used.

About 60% of the sample galaxies have long-exposure X-ray images adequate to detect point-like sources much fainter than ULXs. Short observations were made of the remaining galaxies in the survey using the *Chandra*/ACIS-S detector operating in faint, timed-exposure, mode. These observations were sufficient to *detect* all ULX candidates present in the target host galaxies and to accurately determine their positions, but not deep enough to constrain their X-ray spectral energy distributions in a statistically meaningful way.[6]

3.1. Host Galaxy Properties

Galaxy morphological type, major isophotal angular diameter (measured at surface brightness level 25.0 mag s^{-2} in blue light), major-to-minor isophotal diameter ratio, and position angle (P.A.) were taken from the Third Reference Catalogue of Bright Galaxies (de Vaucouleurs et al. 1991, hereafter RC3). These parameters were used to define a source search region, the "elliptical D_{25}-isophote," for each survey galaxy. Source search regions were overlaid on Digitized Sky Survey blue images of each galaxy to confirm their accuracy. In a few cases, the P.A. or other parameter was clearly in error and adjustments were accordingly made to the region definition. Galaxy center coordinates were taken from the NED.

Figure 1 displays the distribution of the Hubble morphological type of the sample galaxies and of all the galaxies included in the RC3 with tabulated morphological types (12,520 objects). The current sample has a larger fraction of late-type galaxies and smaller fraction of early-type galaxies than the RC3 catalog. This reflects the true scarcity of ellipticals in the Local Volume. (Note that galaxies of uncertain type are cataloged as $T = 0$ galaxies, which explains the large number of these types in the full RC3.)

Distances to target galaxies were taken from the critically assessed values used previously in the ULX catalog of S04. Otherwise, distances were taken from the recent NED compilation of

[6] Superseding deeper observations of a few galaxies have become publicly available since this survey was initiated. They have been used in our analysis instead of our short exposures.

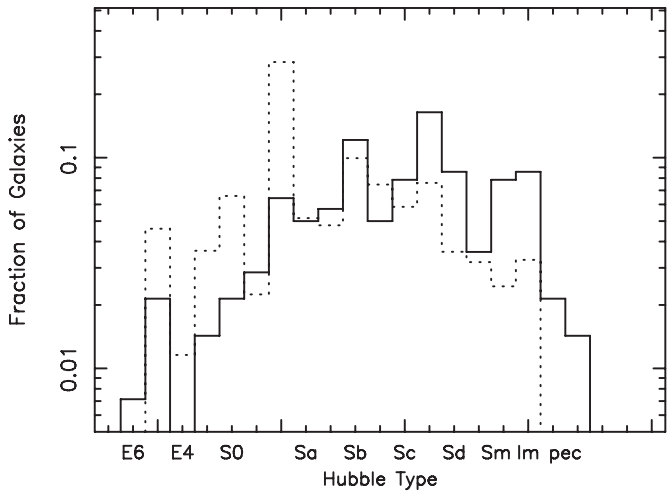

Figure 1. Revised Hubble morphological type, T, of the present sample of galaxies (solid histogram) and of all galaxies in the Third Reference Catalogue (de Vaucouleurs et al. 1991; dotted histogram).

redshift-independent distances[7] in the following order of preference: Cepheid period–luminosity relation from the *Hubble* Key Project results (e.g., Freedman et al. 2001), other Cepheid-based distances, surface brightness fluctuations, the tip of the red giant branch, globular cluster luminosity functions, brightest stars, and the Tully–Fisher relation. Targets not included in the redshift-independent NED compilation or in S04 were assigned distances as listed in the Nearby Galaxies Catalogue (Tully 1988) or, finally, from flow-corrected redshift distances listed in NED, preferring the values corrected for Local Group motions (e.g., Karachentsev & Makarov 1996) over those using only a single-attractor Virgocentric flow model (e.g., Tully & Shaya 1984; see also Mould et al. 2000). In the following, updated distances are used to scale previous results—particularly ULX candidate luminosities.

Total gravitational masses of the sample galaxies were computed from total (asymptotic) B magnitudes corrected for inclination and for Galactic and internal extinction (B_T^0; RC3) using the scaling $\log(M/M_\odot) = -0.4M_B + 2.65$ and distance moduli computed using the distances discussed above. This scaling is the best linear model fit to the 313 galaxies in the Catalog of Neighboring Galaxies (CNG; Karachentsev et al. 2004, hereafter K04) with tabulated masses based on H I rotational velocity curves. This scaling gives an M/L ratio of $2.9\,M_\odot/L_\odot$. Fifty-three of our sample galaxies are included in the subset of CNG galaxies with tabulated masses. A comparison of that tabulation with the above expression shows variations not exceeding 0.5 dex in the logarithm for sample galaxies within this subset.

Galaxy-wide SFRs were estimated from the *IRAS* 60 and 100 μm flux densities using the conversion given in Kennicutt (1998), $\mathrm{SFR}(M_\odot\,\mathrm{yr}^{-1}) = 0.045(L_{\mathrm{FIR}}/10^{42})$, using $L_{\mathrm{FIR}} = 4\pi D^2(1.26\times10^{-11}(2.58S_{60}+S_{100}))$ where S_{60} and S_{100} are the 60 and 100 μm flux densities, respectively (Helou et al. 1985), and D is the distance to the galaxy. The L_{FIR}–SFR relation used here strictly applies to L_{FIR} computed over the broader range 8 μm to 1000 μm which is about $\epsilon \sim 1.7$ times higher (e.g., Rowan-Robinson et al. 1997) than the value estimated here using the standard *IRAS* relation from Helou et al. (1985).

3.2. X-Ray Data Reduction

For *Chandra* observations, ACIS Level 2 event lists were generated by applying a charge transfer inefficiency (CTI) correction to and selecting only standard grades and `status=0` events from Level 1 data using the Chandra Interactive Analysis of Observations (CIAO, version 4.2) software tool `acis_process_events`. For *XMM-Newton* observations, event lists were first calibrated from raw EPIC pn Observation Data Files using Science Analysis System v8.0.0 tool `epchain` to apply gain and CTI corrections. Only events with FLAG = 0 and PATTERN $\leqslant 4$ were used in the analysis. For *ROSAT* observations, HRI or PSPC basic science data event lists were used. In all cases, only events located within the D_{25} isophote were examined in the analysis. An observation identifier is listed in Column 6 of Table 1.

3.3. Source Detections

X-ray sources were located and their celestial coordinates, detected counts, and estimated background within an ∼97% encircled energy radius were tabulated. Details of the source-finding algorithm are given in Tennant (2006). Source-finding was applied to events in the 0.3–6.0 keV range for *Chandra* observations, in the 0.5–4.5 keV range for *XMM-Newton* observations, and in the full 0.1–2.4 keV range for *ROSAT* observations. The different ranges were chosen as those that tend to maximize signal-to-noise ratio (S/N). The durations of the observations were taken from the good time intervals (GTIs) provided as part of the calibrated X-ray event lists. Binned X-ray light curves spanning the duration of the individual observations and covering most or all of the elliptical D_{25}-isophote search region, excluding detected sources, were examined for periods of high background. These time periods were excluded, GTIs recomputed, and source-finding repeated. The aperture-corrected numbers of source counts (within the detection bandpasses) are listed in Column 7 of Table 1. The S/Ns are listed in Column 8.

3.4. Source Positions

The vast majority of the ULX candidates identified in this work have been imaged with *Chandra*'s High Resolution Mirror Assembly. The accuracy of absolute positions in the *Chandra* data have a typical rms systematic error of ∼0.″1 due to uncertainties in the plate scale.[8] Refined estimates of the centroids of the brighter sources were made by fitting an elliptical Gaussian to the spatial distribution of X-ray events. The estimated statistical uncertainty in the source positions due to centroiding errors is less than 0.″2 for *Chandra* observations for a combined single-axis rms error of ∼0.″3. The positional accuracy of sources detected in *XMM-Newton* observations is roughly estimated to be ∼1.″5, those in *ROSAT* observations ∼5″, and the refined estimates are correspondingly larger than those of *Chandra*-imaged sources. Source celestial positions quoted in this work are these centroid-refined positions. They are listed in Columns 1 and 2 of Table 1 and the source's putative host galaxy and distance are given in Columns 3 and 4, respectively.

The radial position of each ULX candidate relative to its host galaxy center, expressed as the fraction, f_{D25}, of the deprojected galaxy radius in units of half the major isophotal diameter, is listed in Column 5 of Table 1.

[7] http://nedwww.ipac.caltech.edu/Library/Distances/

[8] http://asc.harvard.edu/cal/hrma/optaxis/platescale/

Table 1
Properties of ULX Candidates

R.A. (h m s)	Decl. (d m s)	Galaxy	D (Mpc)	f_{D25}[a]	ObsID	cts	S/N	L_{cts}[b] (10^{39} erg s^{-1})	L_X[c] (10^{39} erg s^{-1})	Ref.[d]
01 36 51.08	15 45 46.9	NGC 628	9.7	0.54	2057	354.1	16.5	0.8	2.3	
02 14 04.08	27 52 39.5	NGC 855	9.7	0.11	9550	1032.6	27.4	1.9	2.1	
02 22 31.26	42 19 57.8	NGC 891	10.0	0.16	794	1695.7	36.4	3.9	6.7	
02 22 31.36	42 20 24.4	NGC 891	10.0	0.15	794	2042.7	39.0	4.7	10.4	
02 27 21.52	33 35 00.7	NGC 925	9.1	0.23	7104	96.2	8.6	4.2	...	
02 27 27.53	33 34 43.0	NGC 925	9.1	0.44	7104	458.3	18.5	19.9	24.8	
02 36 23.73	38 59 08.5	IC 239	14.2	0.57	7131	46.3	5.9	2.4	...	
02 36 25.94	38 58 03.6	IC 239	14.2	0.20	7131	31.9	5.1	1.7	...	
02 36 29.75	39 00 14.6	IC 239	14.2	0.91	7131	64.9	7.2	3.4	...	
02 39 09.31	40 52 33.2	NGC 1003	10.6	0.53	7116	45.1	6.0	2.3	...	
02 39 11.66	40 53 13.7	NGC 1003	10.6	0.93	7116	26.5	4.7	1.3	...	
02 39 14.35	30 08 54.7	NGC 1012	14.4	0.18	7133	108.8	9.2	5.7	...	
02 39 14.73	30 08 35.0	NGC 1012	14.4	0.51	7133	21.6	3.8	1.1	...	
02 41 38.79	00 27 36.6	NGC 1055	12.6	0.65	4011	30.5	4.9	1.1	...	
02 42 38.89	−00 00 55.1	NGC 1068	14.4	0.56	344	1407.9	32.1	6.6	31.1	
02 42 39.71	−00 01 01.4	NGC 1068	14.4	0.59	344	528.4	19.5	2.5	2.1	
02 42 40.43	−00 00 52.6	NGC 1068	14.4	0.55	344	221.4	8.6	1.0	6.9	
03 45 55.61	68 04 55.3	IC 342	3.3	0.48	0206890101	...	...	...	11.0	1
03 46 15.64	68 11 12.2	IC 342	3.3	0.60	0206890101	...	...	...	36.0	1
07 36 25.53	65 35 40.0	NGC 2403	3.1	0.37	2014	5649.6	65.5	1.7	2.4	
08 01 48.10	50 43 54.6	NGC 2500	10.1	0.66	7112	110.8	9.2	5.0	...	
08 01 57.85	50 43 39.5	NGC 2500	10.1	0.69	7112	23.3	4.3	1.1	...	
08 14 37.02	49 03 26.6	NGC 2541	11.2	0.35	1635	54.8	6.7	4.2	...	
08 19 29.00	70 42 19.3	UGC 4305	3.4	0.69	1564	2435.7	40.9	6.0	6.0	
09 22 02.22	50 58 54.2	NGC 2841	13.1	0.10	6096	175.5	11.8	1.1	3.0	
09 32 06.16	21 30 58.7	NGC 2903	8.9	0.37	11260	3028.8	49.0	2.8	3.7	
09 55 32.97	69 00 33.4	NGC 3031	3.6	0.30	735	8385.7	76.6	2.5	5.4	
09 55 46.45	69 40 40.3	NGC 3034	3.9	0.10	361	1165.0	29.1	0.6	1.5	
09 55 50.01	69 40 46.0	NGC 3034	3.9	0.04	361	3352.3	48.2	1.7	25.7	
09 55 50.58	69 40 43.2	NGC 3034	3.9	0.03	361	552.0	20.5	0.3	1.9	
09 55 51.16	69 40 43.4	NGC 3034	3.9	0.02	361	1110.8	27.2	0.6	32.9	
09 55 52.13	69 40 53.1	NGC 3034	3.9	0.04	361	764.7	22.9	0.4	2.4	
09 55 54.56	69 41 00.4	NGC 3034	3.9	0.07	361	352.2	15.9	0.2	5.2	
10 18 12.05	41 24 20.7	NGC 3184	14.4	0.42	804	454.0	19.0	2.3	2.8	
10 18 23.00	41 27 41.7	NGC 3184	14.4	0.72	804	515.8	20.0	2.6	3.6	
10 25 06.98	17 09 47.2	NGC 3239	8.1	0.30	7094	31.6	4.8	1.2	...	
10 25 08.20	17 09 48.3	NGC 3239	8.1	0.48	7094	43.5	5.8	1.6	...	
11 01 13.67	03 36 15.6	NGC 3495	12.8	0.66	7126	29.9	4.6	1.4	...	
11 05 45.62	00 00 16.2	NGC 3521	7.2	0.57	9552	2401.9	42.4	1.9	5.2	
11 11 26.05	55 40 16.8	NGC 3556	14.1	0.17	2025	1346.5	32.0	4.6	7.6	
11 11 30.34	55 40 31.3	NGC 3556	14.1	0.08	2025	355.7	16.7	1.2	2.7	
11 11 41.42	55 40 57.8	NGC 3556	14.1	0.42	2025	252.9	13.5	0.9	5.4	
11 18 58.55	13 05 31.0	NGC 3623	7.3	0.45	1637	30.4	4.8	1.0	...	
11 20 15.76	13 35 13.7	NGC 3628	10.0	0.87	2039	2946.7	45.6	14.1	11.9	
11 20 18.32	12 59 00.8	NGC 3627	9.4	0.38	9548	895.1	25.4	1.7	2.6	
11 20 20.90	12 58 46.6	NGC 3627	9.4	0.68	9548	6068.5	65.7	11.4	14.4	
11 20 37.37	13 34 29.2	NGC 3628	10.0	0.61	2918	274.1	14.2	3.5	1.7	2
11 26 07.33	43 34 06.3	NGC 3675	12.8	0.39	396	14.0	3.2	1.4	...	
11 52 37.36	−02 28 07.1	UGC 6850	14.5	0.16	7135	34.7	5.2	1.6	...	
12 06 07.98	47 30 21.2	NGC 4096	8.8	0.84	7103	22.7	4.3	1.1	...	
12 09 22.18	29 55 59.7	NGC 4136	9.7	0.55	2921	352.3	16.0	1.8	2.1	
12 10 33.76	30 23 58.0	NGC 4150	12.8	0.12	1638	55.7	6.6	5.6	...	
12 10 34.77	30 23 58.3	NGC 4150	12.8	0.28	1638	107.7	9.0	10.8	...	
12 15 10.91	20 39 12.4	NGC 4204	7.9	0.59	7092	40.3	5.4	1.4	...	
12 18 43.85	47 17 31.5	NGC 4258	7.7	0.65	1618	403.3	17.6	1.2	1.6	
12 18 57.84	47 16 07.1	NGC 4258	7.7	0.34	1618	856.4	24.5	2.5	5.3	
12 26 01.44	33 31 31.1	NGC 4395	4.2	0.43	402	158.1	10.9	2.4	5.5	
12 28 17.83	44 06 33.9	NGC 4449	3.7	0.45	2031	1439.1	32.8	0.8	1.5	
12 30 29.55	41 39 27.6	NGC 4490	7.8	0.49	1579	276.5	14.4	0.9	19.8	
12 30 30.56	41 41 42.3	NGC 4485	7.8	0.35	1579	2232.7	32.4	7.3	6.3	
12 30 30.82	41 39 11.5	NGC 4490	7.8	0.39	1579	681.8	22.2	2.2	6.5	
12 30 32.27	41 39 18.1	NGC 4490	7.8	0.33	1579	509.4	19.2	1.7	2.9	
12 30 36.32	41 38 37.8	NGC 4490	7.8	0.01	1579	547.2	19.8	1.8	3.5	
12 30 43.26	41 38 18.4	NGC 4490	7.8	0.50	1579	979.3	26.7	3.2	8.3	
12 32 42.83	00 06 53.2	NGC 4517	9.8	0.18	0203170301	...	...	...	10.4	3

Table 1
(Continued)

R.A. (h m s)	Decl. (d m s)	Galaxy	D (Mpc)	f_{D25}[a]	ObsID	cts	S/N	L_{cts}[b] (10^{39} erg s^{-1})	L_X[c] (10^{39} erg s^{-1})	Ref.[d]
12 35 51.71	27 56 04.1	NGC 4559	10.3	0.88	2027	2077.5	39.1	21.4	17.9	
12 35 57.79	27 58 07.4	NGC 4559	10.3	0.16	2027	256.9	14.2	2.6	3.9	
12 35 58.56	27 57 41.9	NGC 4559	10.3	0.10	2027	1392.2	33.0	14.4	16.8	
12 36 08.90	19 19 55.9	NGC 4561	12.3	0.82	7125	53.0	6.3	2.5	...	
12 41 29.14	41 07 57.7	NGC 4618	7.3	0.62	7147	234.3	13.0	1.4	1.8	
12 41 52.72	41 16 31.7	NGC 4625	8.2	0.10	7098	26.2	4.4	1.1	...	
12 41 55.56	32 32 16.9	NGC 4631	7.6	0.34	797	3164.0	47.9	3.2	3.6	
12 42 11.13	32 32 35.9	NGC 4631	7.6	0.10	797	1182.1	30.3	1.2	21.8	
12 50 25.70	25 31 29.8	NGC 4725	11.9	0.33	2976	217.3	12.5	1.3	1.2	
12 50 26.37	25 33 19.4	NGC 4725	11.9	0.71	2976	281.6	14.7	1.7	1.7	
12 50 36.88	25 30 28.4	NGC 4725	11.9	0.54	2976	239.5	13.6	1.4	1.2	
12 50 52.72	41 07 19.0	NGC 4736	5.2	0.02	808	2546.6	43.2	1.5	1.2	
12 50 53.32	41 07 14.0	NGC 4736	5.2	0.01	808	4523.7	56.8	2.7	3.1	
12 55 12.31	00 07 51.9	UGC 8041	14.2	0.58	7132	45.3	6.0	2.1	...	
13 15 19.54	42 03 02.3	NGC 5055	9.2	0.90	2197	2648.6	43.9	8.3	30.4	
13 15 39.33	42 01 53.4	NGC 5055	9.2	0.31	2197	173.5	11.5	0.5	1.4	
13 16 02.27	42 01 53.6	NGC 5055	9.2	0.42	2197	648.5	22.1	2.0	12.2	
13 29 38.61	58 25 05.6	NGC 5204	4.5	0.18	2029	1467.5	32.3	3.4	3.3	
13 29 43.30	47 11 34.8	NGC 5194	8.4	0.46	1622	334.0	15.8	0.9	3.5	
13 29 50.67	47 11 55.2	NGC 5194	8.4	0.12	1622	242.8	13.3	0.7	6.9	
13 29 53.32	47 10 42.7	NGC 5194	8.4	0.21	1622	622.6	21.2	1.7	2.2	
13 29 53.72	47 14 35.7	NGC 5195	8.4	0.67	1622	421.4	18.0	1.2	2.1	
13 29 57.57	47 10 48.6	NGC 5194	8.4	0.24	1622	300.4	15.0	0.8	1.3	
13 30 01.02	47 13 43.9	NGC 5194	8.4	0.59	3932	522.0	20.4	2.6	3.9	
13 30 05.99	47 15 42.3	NGC 5195	8.4	0.41	1622	390.3	16.9	1.1	1.0	
13 30 07.54	47 11 06.1	NGC 5194	8.4	0.69	1622	937.8	26.9	2.6	3.1	
14 03 32.39	54 21 02.9	NGC 5457	7.0	0.21	934	9003.5	73.3	4.7	14.4	
14 04 14.29	54 26 03.8	NGC 5457	7.0	0.76	934	4606.2	59.5	2.4	2.4	
14 04 59.73	53 38 09.1	NGC 5474	6.8	0.68	9546	5161.8	63.3	8.3	14.2	
14 19 39.39	56 41 37.8	NGC 5585	5.7	0.85	7150	243.9	14.0	1.6	2.5	
15 15 58.60	56 18 10.0	NGC 5907	13.4	0.29	0145190101	...	...	...	34.0	4
20 34 36.48	60 09 30.5	NGC 6946	5.5	0.40	1043	941.7	26.6	0.7	3.1	
20 34 52.32	60 09 11.7	NGC 6946	5.5	0.01	1043	837.6	24.7	0.6	2.0	
20 34 56.49	60 08 34.1	NGC 6946	5.5	0.16	1043	406.3	17.8	0.3	3.3	
20 35 00.74	60 11 30.8	NGC 6946	5.5	0.45	1043	9034.0	82.4	6.8	5.7	
20 35 18.79	60 10 56.6	NGC 6946	5.5	0.73	1043	502.4	18.6	0.4	4.5	
21 03 30.08	29 55 15.5	NGC 7013	14.2	0.83	7130	18.4	3.7	1.1	...	
21 03 33.93	29 53 17.8	NGC 7013	14.2	0.34	7130	104.6	9.0	6.5	...	
21 03 35.49	29 52 26.4	NGC 7013	14.2	0.78	7130	23.8	4.4	1.5	...	
22 37 05.64	34 26 53.5	NGC 7331	14.5	0.49	2198	122.7	9.5	1.0	3.2	
22 37 06.61	34 26 20.1	NGC 7331	14.5	0.47	2198	174.6	11.6	1.5	3.7	
22 37 08.08	34 26 00.3	NGC 7331	14.5	0.56	2198	201.1	12.2	1.7	2.4	

Notes.
[a] Radial position within host galaxy expressed as fraction of D_{25} radius.
[b] Unabsorbed 0.3–10.0 keV luminosity estimated from source counts detected in the 0.3–6.0 keV band and assuming an absorbed power-law spectrum of $\Gamma = 1.7$ and a Galactic column density.
[c] Unabsorbed 0.3–10.0 keV luminosity estimated from model fits to the X-ray spectral energy distribution as given by the references in Column 11.
[d] References. (1) Feng & Kaaret 2009; (2) Roberts et al. 2004; (3) Walton et al. 2011a; (4) Sutton et al. 2011.

3.5. Source Luminosities

ULX candidate luminosities were estimated in two ways. First, for all sources, a simple conversion from aperture-corrected observed source counts (in the energy ranges defined above) to luminosities in the 0.3–10.0 keV range was made using the Portable Interactive Multi-Mission Simulator (PIMMS; Mukai 1993). PIMMS estimated the instrument-specific *unabsorbed* (i.e., intrinsic) flux provided the observed source count rate and a model for the spectral energy distribution. An absorbed power-law model was assumed in all cases with an absorption column equal to the line-of-sight Galactic column taken from the H I maps of Kalberla et al. (2005) accessed through the FTOOL utility `nh` and a power-law index fixed at 1.8 following S04.

Second, for sources with >130 counts detected in any observation, either spectral fits were made or published results of spectral fits were taken from the literature. For results taken from the literature, the intrinsic luminosities were converted from the originally published energy range to the 0.3–10.0 keV bandpass and, where needed, scaled to the distances adopted here. PIMMS was used for the bandpass conversion and to scale from observed to intrinsic (unabsorbed) fluxes where needed provided spectral model fit parameters were provided. References to

published spectral modeling results are listed in Column 11 of Table 1.

For sources with >130 detected source counts but without previously published luminosities, spectral analysis was performed using the XSPEC v.11.3.2 spectral-fitting package with redistribution matrices and ancillary response files appropriate to the specific observation. Absorbed (XSPEC's `phabs`) powerlaw (`powerlaw`), blackbody accretion disk (`diskbb`), and optically thin diffuse gas (`apec`) models were applied, sequentially, to the observed spectra until an acceptable fit was obtained according to the χ^2 statistic (events were grouped to ensure a minimum of 10 counts per spectral energy bin). The effects of pile-up of sources with detected count rates in excess of 0.1 counts frame^{-1} in *Chandra*/ACIS observations were treated following the procedures described by Davis (2001) using the multiplicative XSPEC model `pileup`. All ULX candidates in this category, with one exception, were fitted satisfactorily with an absorbed power-law model. The exception is the ULX candidate in NGC 4395 for which no single-component model provided an acceptable fit to the data. The results of the best-fitting ($\chi^2_\nu = 1.16$ for 8 dof) `diskbb` model are quoted in Table 1 for this object. Luminosities were then estimated from the model-predicted unabsorbed flux in the 0.3–10.0 keV energy band and the adopted distance to the ULX candidate host galaxy.

Luminosities estimated from the observed count rates are listed in Column 9 of Table 1 and those estimated from spectral fits or taken from the literature are listed in Column 10.

4. RESULTS OF THE ULX POPULATION CENSUS

4.1. Sample Completeness

ULXs are known to correlate with SFR in late-type galaxies and with stellar mass in early-type galaxies (e.g., S04). How well the current sample of galaxies, and the ULX population it provides, represents a statistically complete inventory can be estimated by measuring the mass and SFR of the sample.

The total dynamical mass in the sample galaxies is estimated, by the methods described in Section 3.1, to be $3.5 \times 10^{12}\,M_\odot$ for a mass density of $5.7 \times 10^8\,M_\odot$ Mpc^{-3} within the sample volume of 6100 Mpc^{-3}. This is slightly less than the density in the Local Volume, $7.3 \times 10^8\,M_\odot$ Mpc^{-3} within 8 Mpc (K04), and slightly more than the mean density measured out to redshifts $z \sim 0.2$ (e.g., Blanton et al. 2003; Liske et al. 2003), $(3.9\text{–}4.2) \times 10^8\,M_\odot$ Mpc^{-3}, assuming $H_o = 73$ km s^{-1} Mpc^{-1} and $M/L = 2.9$ (see Section 3.1). We attribute most of the differences to local variations within our small survey volume and conclude the current survey accounts for most of the mass within the sample volume.

There is, however, a sizable population of nearby dwarf galaxies that are excluded by our selection criteria. Figure 2 compares the masses of galaxies in the current sample to the masses of all galaxies in the CNG (Section 3.1). The CNG is purported to be complete to roughly $B \sim 17$ mag within a distance of ~8 Mpc. The CNG contains a large number of galaxies with masses below about $10^9\,M_\odot$ compared to the sample of galaxies used here. For reference, K04 define dwarfs as galaxies with $M_B > -17$ corresponding to masses $M \lesssim 10^{9.5}\,M_\odot$. However, only about $7 \times 10^{10}\,M_\odot$, or about 4%, of the total mass in the CNG compilation is in dwarf galaxies. A similar mass percentage is likely omitted in the current survey.

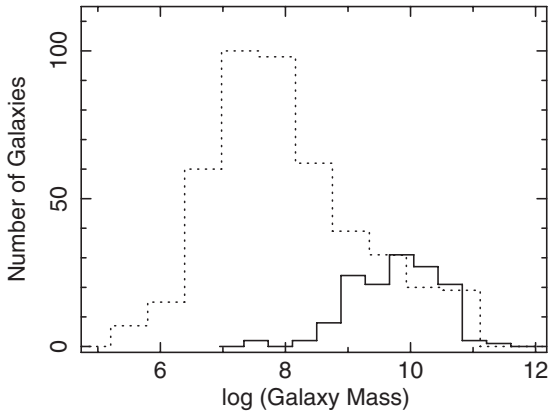

Figure 2. Distribution of estimated masses of galaxies in the present sample (solid histogram) and of all galaxies in the Catalog of Neighboring Galaxies (Karachentsev et al. 2004; dotted histogram). Masses were estimated from absolute B magnitudes as $\log(M/M_\odot) = -0.4M_B + 2.65$ (see the text).

The total SFR in the sample galaxies is $30.3\epsilon\,M_\odot$ yr^{-1} based on their FIR luminosities[9] corresponding to an SFR density of $0.005\epsilon\,M_\odot$ yr^{-1} Mpc^{-3}. As noted in Section 3, these values should be scaled upward by a factor of $\epsilon \sim 1.7$ to account for the full FIR bandpass. The resulting density is then within the range estimated from Hα measurements ($0.013 \pm 0.006\,M_\odot$ yr^{-1} Mpc^{-3}) by Gallego et al. (1995) and from the [O II] SFR indicator ($0.010 \pm 0.005\,M_\odot$ yr^{-1} Mpc^{-3}; Gallego et al. 2002) and just below the Hα estimates by Hanish et al. (2006) of $0.011^{+0.003}_{-0.002}\,M_\odot$ yr^{-1} Mpc^{-3} for nearby galaxies. However, this rate is much less than recent estimates at higher redshifts (e.g., $0.025\,M_\odot$ yr^{-1} Mpc^{-3}, Bothwell et al. 2011; $0.024\,M_\odot$ yr^{-1} Mpc^{-3}, Robotham & Driver 2011, and references therein).

Our selection criteria were designed to sample most major star-forming galaxies but exclude most dwarf galaxies. K04 note that the total H I mass in dwarf galaxies is about 15% of the total amount in their compilation. If H I mass is taken as roughly proportional to SFR (e.g., Kennicutt 1998), then a portion of the total SFR may have been missed in our sample. Swartz et al. (2008) noted that, although ULXs are rare in dwarf galaxies, they do occur at a rate proportional to the SFR and that the SFR per unit mass in dwarf galaxies is higher than in giant spirals.

In summary, the current sample of nearby galaxies is reasonably complete in both mass and SFR. The population undersampled in the survey is the low-mass dwarf galaxies which dominate by number but contribute only a small fraction to the total SFR and an even smaller fraction of the total mass within the sample volume. The potential number of ULXs that may be present in this undersampled population is estimated in the following section.

4.2. The Local ULX Census

There are 107 ULX candidates identified within the current sample of 127 galaxies. Basic properties of these ULX candidates are listed in Table 1. There are thus 0.0175 ULX Mpc^3 in the local universe before correcting for background interlopers and sample incompleteness. From the total estimated mass and SFR for the sample we derive a ULX rate of 1 ULX per 3.2 ×

[9] Here and elsewhere we exclude the SFR contributions from the Seyfert galaxies NGC 1068, NGC 660, and NGC 4826 because their high FIR luminosities are likely dominated by their nuclear activity rather than by star formation.

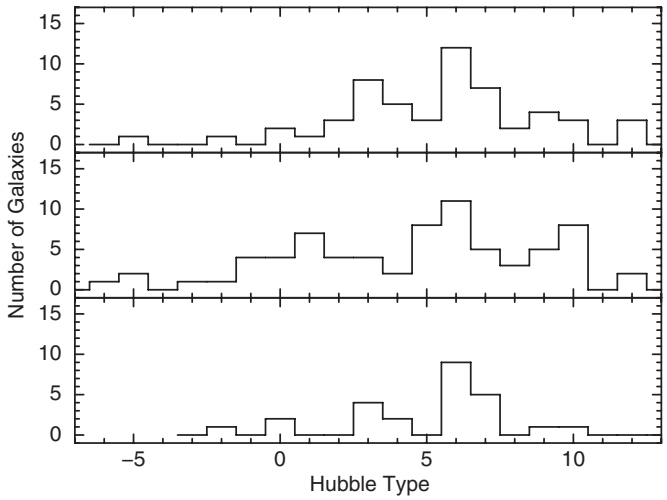

Figure 3. Distribution of revised Hubble types for (top panel) galaxies hosting ULX candidates, (middle panel) galaxies without ULX candidates, and (bottom panel) galaxies hosting ULXs with estimated luminosities in excess of 3×10^{39} erg s^{-1}.

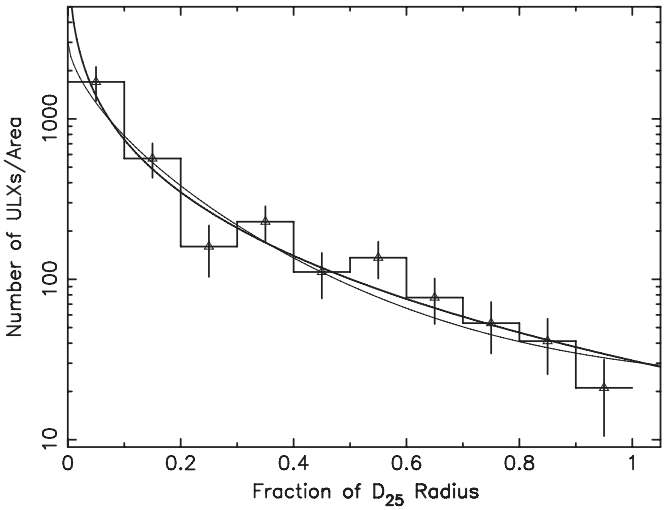

Figure 4. Surface distribution of ULX candidates. The abscissa is the deprojected radial position, f_{D25} (Table 1), expressed as a fraction of the host galaxy's angular radius ($\equiv 0.5D_{25}$) and the ordinate is the number of ULX candidates per unit area fdf, on the range f to $f+df$. The thick curve is the best-fitting generalized exponential, $A\exp(-f/h)^{1/n}$. The best fit is centrally peaked with a value $h \sim 0.001$ and $n \sim 3.6$. The thin curve is the best-fitting function with fixed parameters $h \equiv 0.06$ and $n \equiv 1.6$ corresponding to the best-fit values determined by S04 for a larger sample of 3413 discrete X-ray sources; only the model norm was allowed to vary in determining the thin curve.

$10^{10}\,M_\odot$ and 1 ULX per $0.28\epsilon\,M_\odot$ yr^{-1} SFR (where $\epsilon \sim 1.7$ is the scaling to the full FIR bandpass). Fifty-five of the 127 sample galaxies host ULXs. Galaxies hosting ULXs account for 71% of the total mass in the sample and 83% of the total SFR. If we assume that 85% (following K04) of the actual number of galaxies in the sample volume are dwarf galaxies excluded in the current sample, then there are 850 galaxies in the sample volume and the number of galaxies hosting ULXs is 6.5% of the total by number.

The number of potential background sources included in the search fields can be estimated from the published fits to the 2.0–10.0 keV cosmic X-ray background $\log N - \log S$ distribution (Moretti et al. 2003) as follows. If the 2.0–10.0 keV flux from a ULX of luminosity 10^{39} erg s^{-1} in a galaxy is S (a function of the adopted distance) and the total search area of the galaxy is A, then the expected number of background sources above this flux value is $N(>S) = A/(3.26S^{1.57} + 0.0073S^{0.44})$. Applying this to all galaxies in the present sample results in an estimated 14 background sources. This is a conservative estimate in that the actual cumulative luminosity function for ULXs (Section 4.3) is much flatter than the $\sim S^{-1.57}$ that dominates the background $\log N - \log S$ distribution at fluxes typical of the present study. In fact, by this same analysis, only 0.4, or about 4%, of the ULX candidates more luminous than 10^{40} erg s^{-1} are expected to be background interlopers.

The number of potential ULX candidates within the sample volume hosted by dwarf galaxies, and therefore excluded by our search criteria, can be estimated from the detailed work of Karachentsev et al. (K04) on the Local Volume galaxy population. Assuming the number of ULXs scales with SFR (e.g., Grimm et al. 2003; S04) and that the SFR scales with the H I mass (Kennicutt 1998; but see also, e.g., Kennicutt et al. 2007; Bigiel et al. 2008), then we expect an additional 19 ULXs within the sample volume hosted by dwarf galaxies because the fraction of H I mass contained in dwarf galaxies is 15% according to K04. Assuming that the additional ULXs are distributed among 19 individual dwarf galaxies, then the number of galaxies hosting ULXs (including dwarfs) rises to 8.7% of the total number of galaxies (∼850) in the sample volume. The number of additional ULXs estimated by scaling by mass is less than the uncertainties that can be ascribed to random fluctuations since only 4% of the mass is contained in dwarf galaxies (K04).

As with previous surveys, ULX candidates are found in all galaxy morphological types. Figure 3 displays the distribution of revised Hubble types of galaxies in the sample with no ULXs, those hosting ULXs, and those hosting ULXs more luminous than 3×10^{39} erg s^{-1}. The latter category typically excludes ULXs in elliptical galaxies (Irwin et al. 2004; S04). There are no statistically significant differences among the Hubble type distributions of galaxies with and without ULXs. There are few early-type galaxies hosting ULXs but there are also few early-type galaxies in the sample (cf. also Figure 1). There are more ULXs per late-type ($T > 0$) sample galaxy, 0.48, compared to the rate in ellipticals, 0.23, but this is only a 2σ decrease in the ellipticals compared to the expected value based on the spirals (three observed ULXs and 6.2 ± 2.5 expected in 13 $T \leqslant 0$ galaxies). There is no difference between the number of ULXs per galaxy in early-type spirals ($1 < T < 4$) and in late-type spirals in our sample. Recently, Walton et al. (2011b) found a slight preference for ULXs in early-type spirals but only at the 1σ level. Walton et al. (2011b) did find a higher incidence of ULXs in spirals, 0.59, compared to our sample. This is likely due to the usual bias toward more massive and luminous galaxies inherent in X-ray-selected galaxy samples.

Figure 4 displays the radial distribution of all ULX candidates normalized to their host galaxy deprojected D_{25} isophote radius. The distribution was fitted to a generalized exponential function (Sérsic profile) of the form $A\exp^{-(f_{D25}/h)^{(1/n)}}$. The best-fit parameter values (resulting in the thick curve of Figure 4) approximate a de Vaucouleurs profile, $n = 4$. Fixing the index to $n = 4$ results in a best-fitting scale height $h = 3.0^{+2.4}_{-1.2} \times 10^{-4}$ (90% confidence for one interesting parameter, $\chi^2 = 6.9$ for 8 dof). This indicates a much steeper slope at small values of the abscissa than found previously by S04 for ULXs and for ∼3400 fainter sources, $h = 0.06 \pm 0.03$. Fixing the index to $n = 1.6$ and the scale height to $h = 0.06$, the best-fitting

Table 2
ULX Luminosity Function Fit Parameters

Function	$CL_X^{-\alpha}\exp(-L_X/L_c)$				$CL_X^{-\alpha}$		
	C	α	L_c[a]	ℓ[b]	C	α	ℓ
$N(>L_{sp})$	97.6	0.5	19.7	13.81	103.9	0.8	47.51
$N(>L_{cts})$	103.3	0.9	12.9	5.68	92.9	1.1	14.90
dN/dL_{sp}	$26.3^{+9.8}_{-6.8}$	0.8 ± 0.2	$16.7^{+20.4}_{-6.8}$	5.22	$40.5^{+14.0}_{-11.1}$	1.4 ± 0.2	16.41
dN/dL_{cts}	$78.0^{+124.5}_{-46.7}$	1.6 ± 0.3	$15.2^{+53.0}_{-8.6}$	0.15	92.0 ± 25.0	2.0 ± 0.2	3.61

Notes.
[a] All luminosities are in units of 10^{39} erg s^{-1}.
[b] Maximum likelihood statistic.

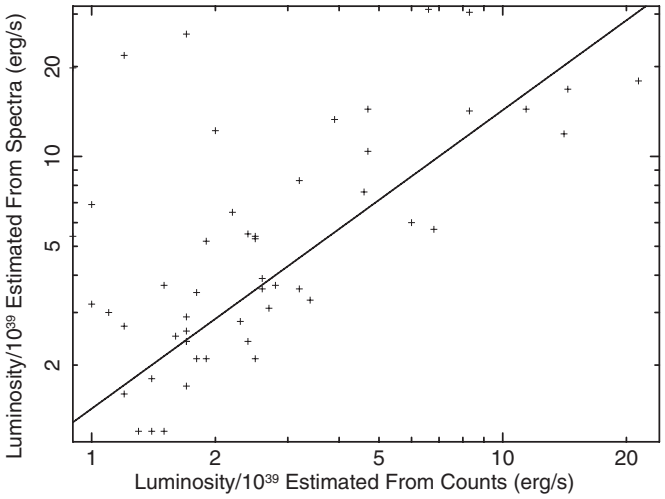

Figure 5. Comparison of intrinsic ULX luminosities estimated from spectral fits and from detected counts. Best-fitting linear function slope is 1.43 showing that luminosities obtained from spectral fits generally exceed luminosities estimated by numbers of detected counts. This is primarily attributable to absorbing column densities estimated by spectral fitting exceeding the line-of-sight Galactic column densities assumed in the calculation of luminosities from detected counts. The scatter of the data is due to differences in fitted spectral shapes (mostly power-law indices but also thermal or other components in some cases) compared to the $\Gamma = 1.8$ power law assumed otherwise.

values found by S04, results in the thin curve shown in Figure 4. Five of the twelve ULX candidates in the range $0 \leqslant f < 0.1$ are within 5″ of their host galaxy nuclei and would have been excluded in our previous survey (S04). No nuclear exclusion region was imposed in the present work. This accounts for some of the steepening of the curve at small values of the abscissa but overall the two curves are similar.

4.3. The ULX Luminosity Function

Table 1 lists estimated intrinsic (absorption-corrected) ULX luminosities based on the detected number of counts and based on fitting models to the observed spectra. Figure 5 shows there are differences between these two estimates. The best linear model fit has a slope of 1.43 meaning that spectroscopically estimated intrinsic luminosities tend to exceed the values estimated from the number of detected counts. This is due primarily to the large column densities derived in the spectral fitting which correlates with a higher estimated intrinsic luminosity compared to the luminosity based on counts which assumes a total column density equal to the Galactic H I column along the line of sight. Column densities of ULX candidates were determined to be, on average, about four times the line-of-sight Galactic column densities by S04. There is also an overall scatter in the luminosity comparison shown in Figure 5. This is due to differences between the modeled spectral shape and the simplistic assumption of a $\Gamma = 1.8$ power law used to estimate luminosities from the detected numbers of counts. While spectroscopic luminosities are preferred as the most accurate estimates, only a subset of the current sample of ULXs have spectroscopic luminosity estimates and the subset is an X-ray-selected subset and hence biased.

With these differences in mind, Figure 6 displays the ULX luminosity function. The upper panels show the integral or cumulative form, $N(>L)$ against L, and the lower panels the differential, dN/dL, luminosity functions. The leftmost panels use spectroscopic luminosities and the rightmost panels the counts-based luminosities. In all cases, two models were fitted to the data: a power law with an exponential cutoff, $CL_X^{-\alpha}\exp(-L_X/L_c)$, and a pure power law, $CL_X^{-\alpha}$, where α is the power-law index, L_c is the cutoff luminosity, and C is the normalization constant. Table 2 records the values of the best-fit parameters for the models. In all cases, a minimum-likelihood fit statistic was used. The formal uncertainties on the model parameters are not given for the cumulative luminosity functions because the data bins in that case are not independent. However, it is clear from the figure that the pure power law is a very poor representation of the data. Note the large formal uncertainties in the differential luminosity function fits due to the strong correlations among the fit parameters even when the fit statistic is near unity indicating an acceptable fit to the data.

The cutoff power-law model provides an improvement over the pure power-law model in all cases. The change in the fit statistic, ℓ, by adding one parameter is 3.46 and 11.19 for the differential luminosity functions based on counts and on spectral fits, respectively, corresponding to 4% and 8% probabilities due to chance alone.

In all cases, the cutoff luminosity is of order 2×10^{40} erg s^{-1} and the (dN/dL) power-law slope is $\sim$1.6, consistent with most values reported previously (e.g., S04; Grimm et al. 2003; Mineo et al. 2011). Walton et al. (2011b) report an acceptable fit (normalized statistic 0.89) from a pure power-law model applied to a sample of 121 ULX candidates. Inspection of their integrated luminosity function, displayed in their Figure 7, reveals a cutoff power law should also provide an acceptable fit to their data. A pure power-law model clearly does not fit our integrated luminosity functions (Figure 6, upper panels) but is an acceptable fit to our differential luminosity functions (Figure 6, lower panels).

The differential luminosity function can also be expressed in terms of the SFR. Following Grimm et al. (2003), we have, for a combined SFR of 51.4 $M_\odot$ yr^{-1} in our sample and a pure power-law representation of the differential luminosity function

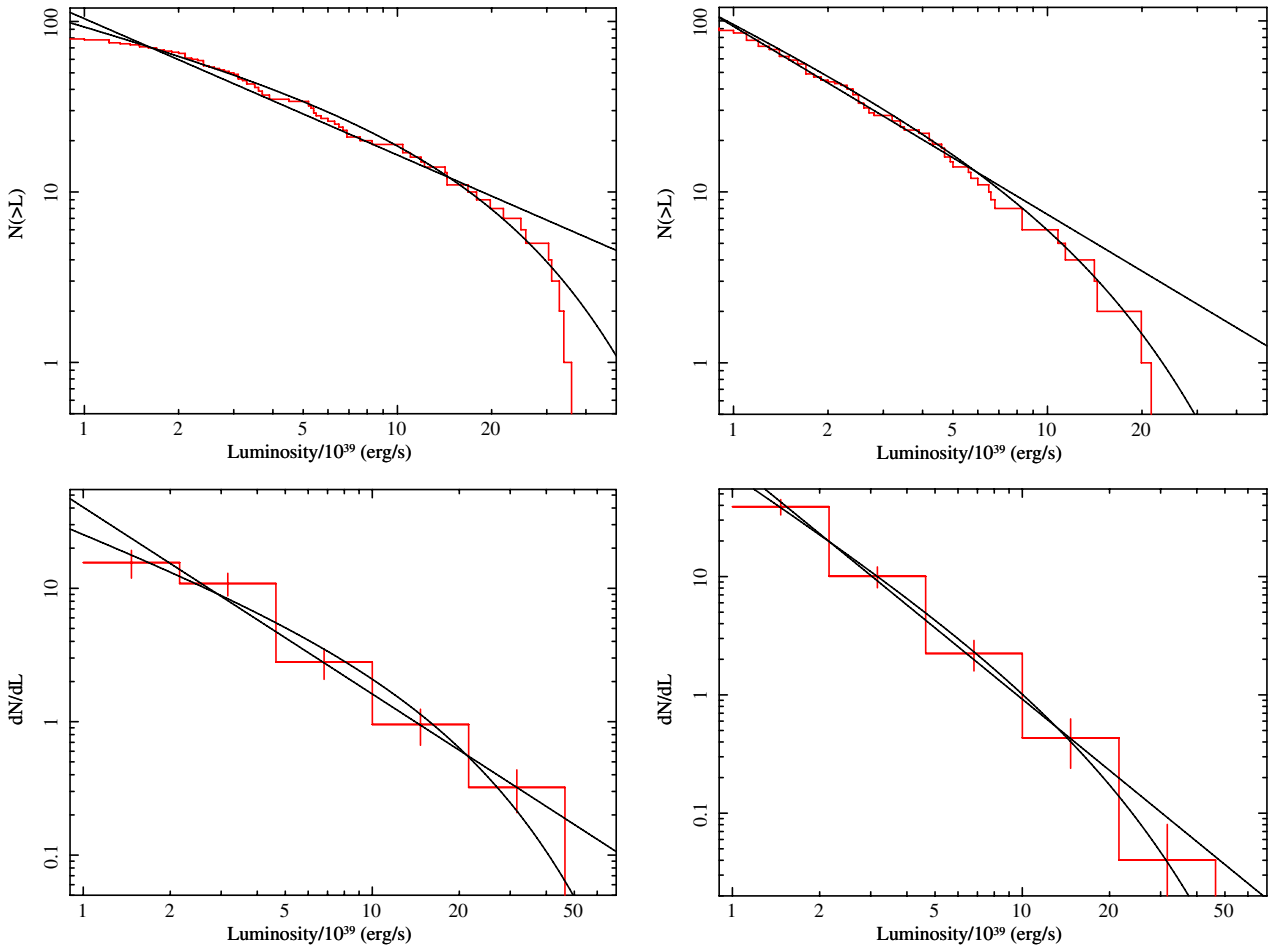

Figure 6. Cumulative (upper panels) and differential (lower panels) ULX luminosity functions using the luminosities estimated from spectral fitting (left panels) and luminosities estimated from the detected number of counts (right panels). Two models were applied in all cases, a power law with an exponential cutoff, $CL_{\rm X}^{-\alpha_1}\exp(-L_{\rm X}/L_c)$, and a pure power-law model, $CL_{\rm X}^{-\alpha_1}$. See Table 2 for model fit parameters.
(A color version of this figure is available in the online journal.)

(Table 2), $dN/dL_{\rm cts} = 1.79 \pm 0.48{\rm SFR}L_{\rm cts}^{-2.0}$ where $L_{\rm cts}$ is in units of 10^{39} erg s^{-1}. Scaling Equation (6) of Grimm et al. (2003) to the same luminosity normalization and accounting for the narrower bandpass, 2–10 keV, over which they estimated luminosities result in an equivalent $dN/dL = 0.6{\rm SFR}L_{\rm cts}^{-1.6}$ for $L < L_c = 21.0$ which indicates that our present census contains roughly twice the number of ULX candidates per unit SFR compared to Grimm et al. (2003). However, we note that applying our FIR-based estimate of the SFR (Section 3.1) to the galaxy sample used to derive Equation (6) of Grimm et al. (2003) results in a 30% reduction in the total SFR compared to their adopted value. This accounts for much of the discrepancy between these two results and suggests that they are roughly consistent.

5. DISCUSSION

A sample of galaxies with known selection criteria has been constructed in order to better quantify the local population of ULX sources and to refine our understanding of the relationships between ULXs, their environments, and other X-ray sources.

We have shown that the sample of galaxies is essentially complete in mass and SFR within a volume of some 6100 Mpc^3 and contains 107 ULX candidates. Within this volume, there is 1 ULX per $3.2 \times 10^{10}\ M_\odot$ and 1 ULX per $0.28\epsilon\ M_\odot$ yr^{-1} SFR where $\epsilon \sim 1.7$.

The ULX number density per unit mass and SFR of their host galaxies are consistent with the extrapolation of the luminosity function of ordinary X-ray binaries (Grimm et al. 2003; Gilfanov 2004). This suggests that most black hole X-ray binaries with luminosities above and below 10^{39} erg s^{-1} originate through similar stellar and binary evolution processes. The ULX subclass is consistent with being the extreme end of this distribution, perhaps in terms of accretion rate and the black hole mass (which can be as high as 80 $M_\odot$ in metal-poor environments; Belczynski et al. 2010). If this is the case, then the onset and duration of the bright X-ray phase in ULXs would also be subject to the same constraints as in ordinary X-ray binaries with the donor star expanding to fill its Roche lobe.

Because of the completeness of the current sample, we can extrapolate the results to somewhat larger volumes to predict properties of the expected population of ULXs more generally. Of particular interest are those objects that are missed in the current sample because they are too rare to appear within random small volumes, namely the very luminous ULXs of which a handful have been recently reported (e.g., Sutton et al. 2011; Farrell et al. 2009).

As luminosity is the defining characteristic of ULXs, the ULX luminosity function can be used to quantify if, indeed, there exists another class of rare high-luminosity objects unrelated to the general ULX population. We can analytically extrapolate

the differential luminosity function from the parameters given in Table 2 and express the results in terms of the volume (or corresponding radius) within which a ULX of a given luminosity would be expected assuming a uniform spatial distribution of ULXs. The cutoff power-law model predicts 1 ULX with a luminosity $L_X/10^{39} > 50, 100,$ and 200 within a radius of 13–29, 42–119, and $\gtrsim$300 Mpc where the low and high end of the quoted ranges corresponds to the differential luminosity functions based on spectral fits and on counts, respectively. This suggests that ULXs with luminosities up to 10^{41} erg s^{-1} can be expected within a distance of $\sim$100 Mpc but that more luminous objects would not be consistent with the population identified here.

Recently, Sutton et al. (2011) described seven high-luminosity ULX candidates, $L_X > 5\times10^{40}$ erg s^{-1}, identified as part of a cross-correlation of the RC3 catalog of galaxies with the second *XMM-Newton* catalog of serendipitously detected X-ray sources from pointed observations (Watson et al. 2009). Using revised distances according to information available from the NED, three of these objects have luminosities below 5×10^{40} erg s^{-1}, including one included in the present sample. Sutton et al. (2011) estimate the luminosities (and distances) to the remaining ULX candidates as, in units of 10^{39} erg s^{-1} (and Mpc): 70 (96.2), 61 (32.8), 103 (32.7), and 270 (95.1). Using the same arguments as above, we expect the numbers of ULXs at (or above) these luminosities and at these distances (within a spherical volume) to be 6.8–105, 2.4–31.8, 0.07–01.92, and $\ll10^{-4}$, respectively. In other words, the existence of the two brightest ULX candidates is inconsistent with expectations. Note that, above our exponential cutoff of a few 10^{40} erg s^{-1}, background sources dominate the candidate source population and this factor is not included in the estimates made in this section. The actual coverage of the 2XMM catalog is 360 deg^2 of the sky (Watson et al. 2009). If we assume that the catalog reaches a uniform depth for the detection of (very luminous) ULXs of $100d_{100}$ Mpc, then the effective volume of the 2XMM catalog is $37000d_{100}^3$ Mpc^3. The corresponding numbers of ULXs expected reduce to 0.09–1.40, 0.20–2.60, 0.006–0.16, and $\ll10^{-4}$.

Farrell et al. (2009) report an object apparently associated with the galaxy ESO 243-49 with a luminosity reaching 1.1×10^{42} erg s^{-1}. Clearly, such a high luminosity is not expected based on the distribution of luminosities reported here. Instead, we may ask if the host galaxy displays any peculiar properties that would be evident in our sample. The galaxy is a large type S0/a edge-on lenticular 90 Mpc distant. Luminous ULXs are not common in early-type galaxies (Irwin et al. 2004; S04; Liu et al. 2006). The galaxy is not detected in *IRAS* images, which places a conservative upper limit to its SFR of $\sim3\,M_\odot$ yr^{-1}, but, because it is an early-type galaxy and viewed edge-on (which tends to enhance IR emission related to disk star formation and nuclear activity), its actual SFR is likely much lower and therefore unlikely to host luminous ULXs (Grimm et al. 2003; S04). However, it is a large massive galaxy ($M_B = -19.85$; $\log(M/M_\odot) = 10.6$) that would likely be detectable by *IRAS* were it located within our sample volume and it would be well within our other selection criteria for angular size and photographic brightness. Finally, the ULX candidate is located in the halo of ESO 243-49 which is an unlikely location for a ULX (Swartz 2006). In summary, a new class of object is needed to account for ULXs such as ESO 243-49 HLX-1 and for any ULX in excess of $\sim2 \times 10^{41}$ erg s^{-1} in the local universe.

REFERENCES

Abramowicz, M. A., Czerny, B., Lasota, J. P., & Szuszkiewicz, E. 1988, ApJ, 332, 646
Baumgardt, H., Hopman, C., Portegies Zwart, S., & Makino, J. 2006, MNRAS, 372, 467
Beichman, C. A., Neugebauer, G., Habing, H. J., Clegg, P. E., & Chester, T. J. 1988, NASA RP-1190 (Washington, DC: GPO)
Belczynski, K., Bulik, T., Fryer, C. L., et al. 2010, ApJ, 714, 1217
Bigiel, F., Leroy, A., Walter, F., et al. 2008, AJ, 136, 2846
Blanton, M. R., Hogg, D. W., Bahcall, N. A., et al. 2003, ApJ, 592, 819
Bothwell, M. S., Kennicutt, R. C., Johnson, B. D., et al. 2011, MNRAS, 415, 1815
Davis, J. E. 2001, ApJ, 562, 575
de Vaucouleurs, G., de Vaucouleurs, A., Corwin, H. G., Jr., et al. 1991, Third Reference Catalogue of Bright Galaxies (Berlin: Springer)
Farrell, S. A., Webb, N. A., Barret, D., Godet, O., & Rodrigues, J. M. 2009, Nature, 460, 73
Feng, H., & Kaaret, P. 2009, ApJ, 696, 1712
Freedman, W. L., Madore, B. F., Gibson, B. K., et al. 2001, ApJ, 553, 47
Gallego, J., García-Dabó, C. E., Zamorano, J., Aragón-Salamanca, A., & Rego, M. 2002, ApJ, 570, L1
Gallego, J., Zamorano, J., Aragon-Salamanca, A., & Rego, M. 1995, ApJ, 455, L1
Gilfanov, M. 2004, MNRAS, 349, 146
Gladstone, J. C., Roberts, T. P., & Done, C. 2009, MNRAS, 397, 1836
Grimm, H.-J., Gilfanov, M., & Sunyaev, R. 2003, MNRAS, 339, 793
Hanish, D. J., Meurer, G. R., Ferguson, H. C., et al. 2006, ApJ, 649, 150
Helou, G., Soifer, B. T., & Rowan-Robinson, M. 1985, ApJ, 298, L7
Irwin, J. A., Bregman, J. N., & Athey, A. E. 2004, ApJ, 601, L143
Kalberla, P. M. W., Burton, W. B., Hartmann, D., et al. 2005, A&A, 440, 775
Karachentsev, I. D., Karachentseva, V. E., Huchtneier, W. K., & Makarov, D. L. 2004, AJ, 127, 2031
Karachentsev, I. D., & Makarov, D. A. 1996, AJ, 111, 794
Kawaguchi, T. 2003, ApJ, 593, 69
Kennicutt, R. C., Jr. 1998, ARA&A, 36, 189
Kennicutt, R. C., Jr., Calzetti, D., Walter, F., et al. 2007, ApJ, 671, 333
King, A. R. 2009, MNRAS, 393, L41
King, A. R., & Dehnen, W. 2005, MNRAS, 357, 275
Liske, J., Lemon, D. J., Driver, S. P., Cross, N. J. G., & Couch, W. J. 2003, MNRAS, 344, 307
Liu, J.-F., Bregman, J. N., & Irwin, J. 2006, ApJ, 642, 171
Madau, P., & Rees, M. J. 2001, ApJ, 551, L27
Madhusudhan, N., Justham, S., Nelson, L., et al. 2006, ApJ, 640, 918
Mineo, S., Gilfanov, M., & Sunyaev, R. 2011, arXiv:1105.4610
Moretti, A., Campana, S., Lazzati, D., & Tagliaferri, G. 2003, ApJ, 588, 696
Mould, J. R., Huchra, J. P., Freedman, W. L., et al. 2000, ApJ, 529, 786
Mukai, K. 1993, Legacy, 3, 21
Nilson, P. 1973, Uppsala General Catalogue of Galaxies (Acta Universitatis Upsaliensis. Nova Acta Regiae Societatis Scientiarum Upsaliensis—Uppsala Astronomiska Observatoriums Annaler, Uppsala: Astronomiska Observatorium)
Perna, R., Soria, R., Pooley, D., & Stella, L. 2008, MNRAS, 384, 1638
Perna, R., & Stella, L. 2004, ApJ, 615, 222
Portegies Zwart, S. F., Baumgardt, H., Hut, P., Makino, J., & McMillan, S. L. W. 2004, Nature, 428, 724
Poutanen, J., Lipunova, G., Fabrika, S., Butkevich, A. G., & Abolmasov, P. 2007, MNRAS, 377, 1187
Ranalli, P., Comastri, A., & Setti, G. 2003, A&A, 399, 39
Roberts, T. P., Warwick, R. S., Ward, M. J., & Goad, M. R. 2004, MNRAS, 349, 1193
Robotham, A. S. G., & Driver, S. P. 2011, MNRAS, 413, 2570
Rowan-Robinson, M., Mann, R. G., Oliver, S. J., et al. 1997, MNRAS, 289, 490
Sutton, A. D., Roberts, T. P., & Walton, D. J. 2011, Astron. Nachr., 332, 362
Swartz, D. A. 2006, ApJ, 651, L21
Swartz, D. A., Ghosh, K. K., Tennant, A. F., & Wu, K. 2004, ApJS, 154, 519
Swartz, D. A., Soria, R., & Tennant, A. F. 2008, ApJ, 684, 282
Tennant, A. F. 2006, AJ, 132, 1372
Tully, R. B. 1988, Nearby Galaxies Catalogue (Cambridge: Cambridge Univ. Press)
Tully, R. B., & Shaya, E. J. 1984, ApJ, 281, 31
Walton, D. J., Gladstone, J. C., Roberts, T. P., et al. 2011a, MNRAS, 414, 1011
Walton, D. J., Roberts, T. P., Mateos, S., & Heard, V. 2011b, arXiv:1106.0197
Watson, M. G., Schröder, A. C., Fyfe, D., et al. 2009, A&A, 493, 339